Chapter 2

Computational Details

We summarise all computational details of the calculation methods for simulations and modelling approaches chapter by chapter, indicating the program packages used. In particular, the most important steps for the multiscale model as implemented in the charge transport program packages are presented.

2.1 Charge Transfer Rates

The wavefunction and geometry optimisations were performed with the Gaussian 09 Rev. D.01 program package (G09) [251]. For the calculation of the charge transfer integrals and the internal reorganization energy λ^{in} in P3HT, the polymer chains are reduced to the polymer backbone, substituting the hexyl side chains by methyl groups, leading to poly(3-methylthiophene) (P3MT).

Charge transfer integrals Charge transfer integrals were calculated using the different methods introduced in section 1.4.3, e.g. CDFT, DIPRO, ZINDO/MOO. All CDFT-based intermolecular and intramolecular charge transfer integrals [113, 114, 116] were calculated with the CPMD software package [252] using the PBE functional [100] in conjunction with Troullier-Martins norm-conserving pseudopotentials [168] and a plane wave (PW) basis set truncated at an energy cutoff of 80 Ry.

For a DIPBI dimer, an orthorhombic simulation box of size $22.0 \times 21.0 \times 25.0$ Å^3 was chosen. For homo-molecular P3MT pairs, the box size was adjusted according to their conformation — from $15.0 \times 13.0 \times 23.0$ Å^3 to $15.0 \times 16.0 \times 23.0$ Å^3 for P3MT 3mers, from 15.0Å$\times 16.0 \times 23.0$ Å^3 to $15.0 \times 16.0 \times 30.0$ Å^3 for P3MT 5mers, and from $15.0 \times 13.0 \times 35.0$ Å^3 to $15.0 \times 16.0 \times 39.0$ Å^3 for P3MT 7mers.

An in-house code was developed to perform DIPRO calculations using orbitals generated by the Gaussian 09 or DFTB+ [253] programs. DIPRO charge transfer integrals were calculated in combination with the semiempirical PM3 [156, 254, 255], AM1 [155], ZINDO [157, 158], and DFTB [141, 143] methods, as well as with DFT. In the Gaussian 09 package, the DFTB calculations are performed with Slater-Koster files [144,145] and the Mio-1-1 [256, 257] parametrisation, while the DFTB+ program package uses the self-consistent-charge density-functional tight-binding method (SCC-DFTB) [142] approach with the 3OB-3-1 set of parameters for the third-order parametrisation for organic and biological systems [258–260]. DIPRO/DFT calculations were carried out with the exchange-correlation functionals PBE [100], PBE0 [101], and B3LYP [102] in combination with the basis sets 6-31G* or 6-311G**.

The charge transfer integrals with the ZINDO/MOO method [214] were computed using the VOTCA program package [57,213]. We provide a single orbital file with MO coefficients from a ZINDO calculation (G09) for each species.

Reorganization energy and internal site-energy difference The determination of reorganization energies λ^{in} and $\lambda^{\text{in}}_{\text{ONIOM}}$, and the site-energy differences ΔE^{in} are implemented as an on-the-fly method in the charge transport program package, which performs Gaussian 09 calculations using a four point scheme (Fig. 1.2).

The internal reorganization energy and the internal site-energy difference are evaluated using both the B3LYP functional [98, 99] with the 6-311G** basis set [153, 160, 163] and DFTB in combination with the Mio-1-1 parameter set for DIPBI and P3MT with different lengths $n \in [1, 32]$.

We employ a three layer approach ONIOM(QM/MM/PCM) [261,262] for the reorganization energy $\lambda^{\text{in}}_{\text{ONIOM}}$ inside a cavity. The QM region is treated on PBE0/6-31G* (P3MT) or B3LYP/6-31G* (DIPBI) level of theory, the UFF model is applied to the surrounding MM region and embedded into third PCM layer. The PCM layer is modelled by a dielectric permittivity for P3HT for high frequencies ε_{opt}=3.0 [263] and at low frequencies ε_{s} =3.5 [264] determine and using scaled Van der Waals radii with the Bondi model for the cavity [265]. The partial charges are determined for P3HT all thiophene segment length $n \in [1, 32]$ with the CHelpG method [233] on PBE0/6-31G* level. Therefore, we average for every n, and all three charged states c the partial charges of 10 randomly selected geometries from the atomistic morphology. The use of an electronic embedding allows the inclusion of partial charges from the MM region into the QM Hamiltonian.

Outer-sphere Contributions The outer-sphere reorganization energy contributions λ^{out} were evaluated taking into account all atoms inside the simulation box using the minimum image convention [57]. The Pekar factor [228,229] was estimated to be $c_p = 0.05$ from the experimentally determined dielectric permittivity of P3HT at high frequencies, ε_{opt}=3.0, [263] and at low frequencies, ε_{s} =3.5, [264]. In the absence of any corresponding data for DIPBI, we approximated the c_p value of the blend with that of pure P3HT.

The outer-sphere contributions E^{out} to the site-energy difference, E^{el} and E^{pol} (see Sec. 1.4.4), were evaluated in a self-consistent fashion using the Thole model [231, 237] with a default cutoff of about $r^{\text{out}}_{\text{cut}} = 30$ Å [57], using atomic polarisabilities and partial charges. The set of (unscaled) atomic polarizabilities $\alpha_{\text{H,C,N,O,S,Cl}} = (0.496, 1.334, 1.073, 0.837, 2.926, 1.504)$ Å^3 is employed within the Thole model [231, 237] for all atomic species as a default. Moreover, we apply a damping factor of $a = 0.39$ for interactions with induced moments to avoid a polarisation catastrophe [266].

The partial charges were obtained with Gaussian 09, using the CHelpG method [233] with DFT/B3LYP/6-311G** by averaging over 10 samples of the same species extracted from the atomistic morphology for its neutral, positively or negatively charged state, respectively. This procedure is used for DIPBI and for both P3HT and P3MT segments of different length $n \in [1, 32]$.

We use the GDMA program provided by A. J. Stone [236] to perform a gaussian distributed multipole analysis (GDMA) of wave functions based on SCF calculations using DFT/B3LYP/6-311G** in Gaussian 09. This yields a set of multipole moments at the atomic nuclei positions to describe the electrostatic field of each molecular species. The GDMA files (.mps) are provided for each species in all three charged states to determine the outer-sphere contributions using VOTCA.

2.2 Charge Transport in Organic Solar Cells

2.2.1 Workflow of the Multiscale Model

This thesis includes an in-house implementation of a charge transport package. The *charge_transport_package* [267] is provided as a GitHub repository together with data to evaluate charge transfer rates and to perform kMC simulations. It is written in Fortran 90, Python, and combined with Bash shell scripts. It has interfaces to quantum chemistry software packages. The main options are provided by an options.xml file using XML tags.

An overview of the main steps in the workflow is shown in Figure 2.1. A single frame extracted from the atomistic morphology based on GROMACS [268, 269] calculations is partitioned into hopping sites. The sites represent the charge localisation on individual molecules or polymer segments. They are saturated with hydrogen atoms, and a topology file is written, which decodes the exact sequence of single molecules and polymer segments for each MD frame, individually. A list of charge transfer pairs AB is determined.

The package basically provides input files for subsequent calculations on pair properties using program packages as CPMD [252], Gaussian09 (G09) [251], DFTB+ [253], VOTCA [57,213] and runs the calculations on high-performance computing facilities. For instance, the DIPRO calculations require for every pair two electronic structure calculations on each monomer and one on the dimer structure. The required output data is collected, and the intermolecular $|J_{\mathrm{AB}}|$ is determined (see Sec. 1.4.3.1). In contrast, we employ only a single pre-optimised geometry for each specimen in the system as a reference geometry and in each electronic state (n, e, h). We either calculate the electrostatic potential with the CHelpG method [233] in conjugation with DFT to obtain the partial charges q^n, q^e, q^h, or we use the GDMA program by A. Stone [235] to get the multipole moments Q^a_{kl} in combination with atomic polarisabilities $\boldsymbol{\alpha}$. The charge transport package feds this reference data into VOTCA and controls the workflow to determine $\lambda^{\mathrm{out}}_{\mathrm{AB}}$ and $\Delta E^{\mathrm{out}}_{\mathrm{AB}}$, which we use as a standard procedure. Alternatively, the charge transport package can evaluate $\lambda^{\mathrm{out}}_{\mathrm{AB}}$ and $\Delta E^{\mathrm{out}}_{\mathrm{AB}}$ using the expressions (Eq. 231), (Eq. 233) and (Eq. 234) employing the atomic positions of molecules within the environment of a spherical cutoff radius or the entire box. Accordingly, we evaluate other quantities as $|J^{\mathrm{int}}_{\mathrm{AB}}|$, $\lambda^{\mathrm{in}}_{\mathrm{AB}}$ and $\Delta E^{\mathrm{in}}_{\mathrm{AB}}$. The details are presented in Sec. 2.1. The charge transport package collects all required physical components to determine the charge transfer rates (Marcus, Jortner, Weiss-Dorsey) and stores the data in a SQL database. Several properties are also stored in mapping files, e.g. the internal reorganization energy, the path to reference coordinate and orbital files, identification numbers of frontier orbital for HOMO and LUMO, the path to multipole files for the neutral, positively, and negatively charged molecule, and the information of mapping the QM to MM coordinates including atomic weights, and the virtual site assignment. Thus, the mapping file (system.xml) provides a collection of molecule-specific data for each species.

KMC simulations are performed in the charge transport package or in VOTCA based on *a priori* evaluated network of rates k_{AB}. Alternatively, kMC simulations that determine the rates k_{AB} in an *on the fly* modus have the advantage that molecular configurations can be updated according to the molecular dynamics trajectory (See Python program [78]). A Bash shell script aids to scan free parameters, e.g. T and $\mathbf{F}^{\mathrm{ext}}$, and supports performing multiple kMC simulations simultaneously using GNU parallel [270]. The network of rates k_{AB} between nodes with averaged occupation numbers p^{occ} is transformed into a network of local resistances $R^{\mathrm{loc}}_{\mathrm{AB}}$. Finally, the implemented Dijkstra's algorithm [73] finds pathways of low resistance crossing the simulation box. Hence, the charge transport package gives access to macroscopic properties like $\boldsymbol{\mu}$, $\boldsymbol{I}$, and R.

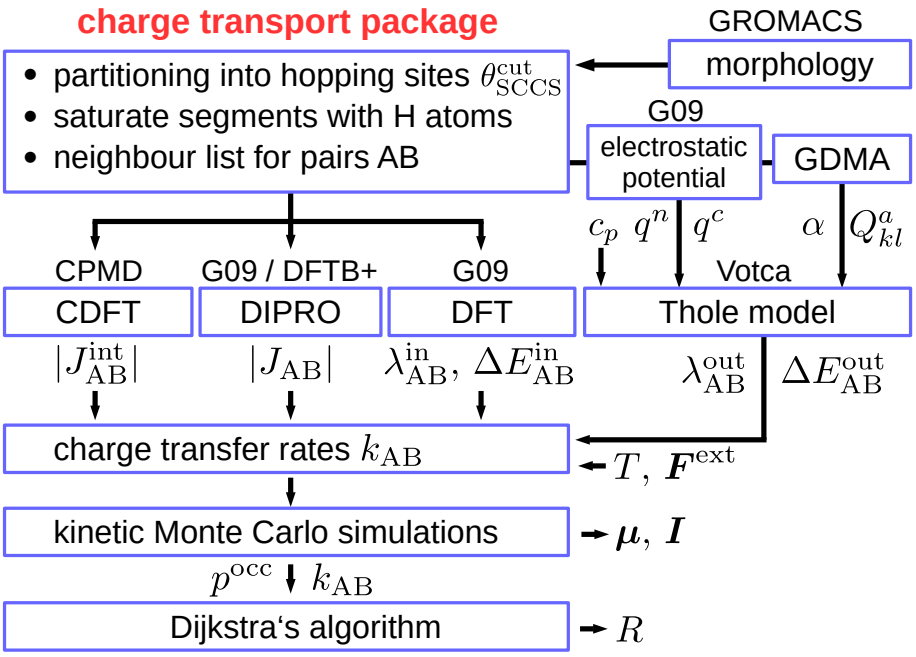

Figure 2.1: Workflow for microscopic simulations of charge transport using the in-house charge transport package combined with GROMACS, G09, DFTB+, CPMD, VOTCA, GDMA.

2.2.2 P3HT and P3HT:DIPBI

Morphology Atomistic molecular mechanics (MM) simulations are performed using the GROMACS program package [268,269]. We use an initial, amorphous P3HT morphology published elsewhere [69] with 416 P3HT polymer chains with $n = 32$ thiophene rings. It is reheated to $T = 900$ K for 15 ns in a NPT run with a velocity rescale thermostat [180], a Parrinello-Rahman barostat [271] with a constant pressure of $p = 1$ bar and a time step of $\Delta t = 1$ fs. Subsequently, the system is cooled to $T = 300$ K and run for 1 ns, resulting in a unit cell with an average dimension of $(30.6 \times 10.4 \times 10.5\ \text{nm}^3)$.

The blend simulations are performed in an orthorhombic box of size $13.9 \times 26.9 \times 14.6\ \text{nm}^3$, containing 416 P3HT polymers made up of 32 thiophene units, each, and 1248 DIPBI molecules, corresponding to a density of $\varrho = 1.245\ \text{g/cm}^3$. We focus on three different morphologies, which were equilibrated in coarse grained molecular dynamics runs at $T =$ 500 K, 700 K, and 900 K, followed by a backmapping to an atomistic MM representation and re-equilibration at room temperature [64].

The angle density to distance plot was generated with the Molecular Plane Analyser package [272], where the distance and orientation analysis of DIPBI molecules in P3HT:DIPBI was carried out with an intermolecular cutoff distance of 15 Å.

Charge Transport Simulations The hopping rates are calculated for the 12 nearest neighbours of every hopping site, defined by the distance of the centre of mass (COM) in nearest image convention in the orthorhombic simulation box. This corresponds to an average distance of the twelfth neighbour of $\overline{d}^{\text{P3HT}}_{\text{NN12}} = (10.8 \pm 1.6)$ Å for P3HT hopping sites and $\overline{d}^{\text{DIPBI}}_{\text{NN12}} = (14.5 \pm 1.6)$ Å for DIPBI, and leads to a average distance between the hopping sites of $\overline{d}_{\text{AB}} = (8.4 \pm 3.1)$ Å (Tab. A.3).

The kMC simulations are based on a set of precomputed charge transfer rates, and they are carried out with the VOTCA program package [57,213]. As a default, we apply a moderate external field of magnitude $|F^{\text{ext}}| = 1.0 \times 10^7$ V/m [57,273] in x, y, or z direction and average over $N_{\text{kmc}} = 72$ kMC simulations per field direction with $N_{\text{steps}} = 1.0 \times 10^{10}$ steps, each, of a single charge carrier inside the simulation box to obtain the total mobility $\mu_{\text{tot}} = \sqrt{\mu_{\text{x}}^2 + \mu_{\text{y}}^2 + \mu_{\text{z}}^2}$ at a temperature $T = 300$ K.

The kMC simulations are initialized as follows. At the beginning of every simulation, a single morphology frame is extracted from the atomistic P3HT:DIPBI MM simulation and partitioned into hopping sites. Each DIPBI molecule is regarded as a single hopping site, due to its extended frontier π-orbitals, whereas the P3HT 32mer chains are separated into subunits according to the torsional angle between the individual thiophene rings. If the dihedral angle θ_{SCCS} between two adjacent rings meets the cutoff criterion,

$$\begin{aligned} \theta_{\text{SCCS}} &\in [\theta_{\text{SCCS}}^{\text{cut}}, 180^\circ - \theta_{\text{SCCS}}^{\text{cut}}] \text{ or} \\ \theta_{\text{SCCS}} &\in [-\theta_{\text{SCCS}}^{\text{cut}}, -180^\circ + \theta_{\text{SCCS}}^{\text{cut}}], \end{aligned} \tag{268}$$

the rings are considered to belong to different hopping sites in the polymer chain. A cutoff dihedral angle of $\theta_{\text{SCCS}}^{\text{cut}} = 75^\circ$ was chosen for the SCCS dihedral angle θ_{SCCS} between two adjacent thiophene rings [69] (for more details, see Sec. 3.1.2).

This procedure results in hopping sites corresponding to polymer segments of different lengths $n \in [1, 32]$ (Fig. 2.2). The distribution of the number of segments with a certain chain length distribution n are similar for the P3HT:DIPBI blend morphologies when comparing different annealing schemes (500 K, 700 K, 900 K). We find hopping sites with a segment length between $n = 1$ and 16 in the blend, whereas, segments with $n = 1$ to 32 can occur in amorphous P3HT.

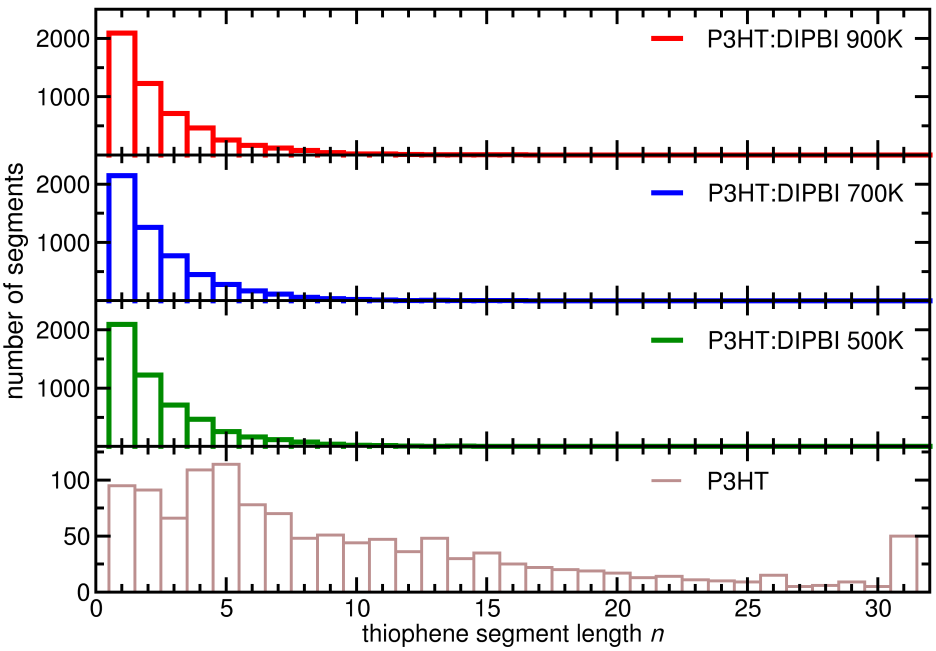

Figure 2.2: Distributions of the number of segments with a certain chain length distribution n for the P3HT:DIPBI blend after employing the polymer chain partitioning with $\theta_{\text{SCCS}}^{\text{cut}} = 75^\circ$ in three different morphologies and CG annealing protocols [64] at 500 K, 700 K and 900 K in amorphous P3HT for comparison.

For the P3HT morphology, we thus arrive at $N_{\text{sites}} = 1284$ hopping sites, yielding $N_{\text{pairs}} = 9985$ charge transfer pairs in the neighbour list, including $N_{\text{int}} = 878$ intrachain transitions. For the P3HT:DIPBI blend morphology at 500 K, one obtains a total of 47546 hopping pairs, composed of 3496 DIPBI↔DIPBI, 8726 DIPBI↔P3HT, and 35324 P3HT↔P3HT hopping pairs. The latter category is subdivided into 4851 intrachain and 30473 interchain transition between hopping pairs. A similar partitioning is obtained for the morphologies at 700 K and 900 K (Tab. A.3).

As the employed atomistic force field includes united atom types, the molecules need to be saturated with H atoms at the aliphatic side chains prior to the quantum-chemical calculations. This also applies to the boundaries between intrachain P3HT segments, where additional H atoms are inserted to saturate the segments to be able to perform DIPRO charge transfer integral calculations. These H atoms are afterwards treated as virtual H atoms in the multipole expansion schemes and do not contribute to the outer-sphere energy contributions. All intermolecular and intramolecular charge transfer rates are pre-evaluated for all pairs in a neighbour list and loaded into the VOTCA program package to perform the kMC simulations.

Nearest neighbours The kMC algorithm requires the evaluation of charge transfer rates for neighbouring hopping pairs. As the charge transfer integral decays exponentially with increasing intermolecular distance, the rates drop to zero numerically at large hopping site distances $\mathbf{d}_{\text{AB}}$. Hence, we do not need to evaluate all possible combinations of charge transfer pairs inside the morphology, but we can limit the evaluation to a number of nearest neighbours (NN) N^{NN}, provided that the total escape rate k^{esc} remains basically constant as N^{NN} rises. The selection of possible neighbours is limited by a cutoff for the number of neighbours $N_{\text{cut}}^{\text{NN}}$ in combination with the RCOM (Eq. 280) distance criterion. We apply an implementation [78] of the grid search algorithm to determine the NN [268]. Alternatively, if we use the implementation in VOTCA, the COM distance (Eq. 275) is employed, including the neighbours around a hopping site within a sphere with a cutoff radius $r_{\text{cut}}^{\text{NN}}$.

In general, we use the convention to evaluate the charge transfer rates to the $N_{\text{cut}}^{\text{NN}} = 12$ nearest neighbours of each hopping site, which includes roughly the same neighbours as selected by a sphere with cutoff radius $r_{\text{cut}}^{\text{NN}} \approx 15$ Å. A motivation for this practice is provided in Sec. A.1.5.

2.2.3 PPDI

We study an amorphous morphology containing 800 PPDI molecules. The simulation box is $(11.7 \times 10.8 \times 10.7)$ nm^3. The kMC simulations are performed with the VOTCA program package [57, 213]. The $|J_{\text{AB}}|$ are based on ZINDO/MOO [157, 214], and λ^{in} on B3LYP/6-311G** level of theory. The outer-sphere contributions to the site-energy difference, E^{el} (Eq. 235) and E^{pol} (Eq. 241), were calculated in a self-consistent fashion using the Thole model [231, 237] with a default cutoff $r_{\text{cut}}^{\text{out}} = 30$ Å [57]. We use the (unscaled) atomic polarizabilities $\alpha_{\text{H,C,N,O}}$ as listed above [237]. The required partial charges were determined using G09 [251] with the CHelpG method [233] with DFT B3LYP/6-311G** by averaging over 10 PPDI molecules extracted from the atomistic morphology for its neutral, positively or negatively charged state, respectively. The external field is applied with a magnitude $\mathbf{F}_l^{\text{ext}} = 1.0 \times 10^7$ V/m with l in x, y, z direction, and the total field-effect mobility is averaged. The mobility is converged for every configuration with $N_{\text{traj}} = 140$ single charge carrier kMC trajectories and $N_{\text{steps}} = 1 \times 10^{10}$ simulation steps each.

2.2.4 PBDT-TS1:PPDI

The morphology contains 464 PBDT-TS1 polymer chains and 1792 PPDI molecules. The PBDT-TS1:PPDI was obtained by atomistic molecular mechanics simulations at an annealing temperature $T = 900$ K for a simulation time $t = 35$ ns with a time step $\Delta t = 1$ fs. After these simulations in NPT ensemble at a constant pressure $p = 1$ bar, the system was cooled back to 300 K for 5 ns. The simulation box is $(16.5 \times 22.0 \times 19.5)$ nm^3. The force field development and the MM simulations were carried out by Thorsten Winands.

The PBDT-TS1 polymer consists of eight repetitive monomeric units, which are made up of two subunits, the thieno[3,4-b]thiophene-based subunit (**A**) and the PBDT subunit (**B**) (Fig. 2.3). The labels (**A**) and (**B**) are introduced to facilitate the polymer sequence assignment. We distinguish two SCCS-cutoff angles θ(**AB**) and θ(**BA**) as possible segment delimiters between the subunits in the subsequent kMC simulations.

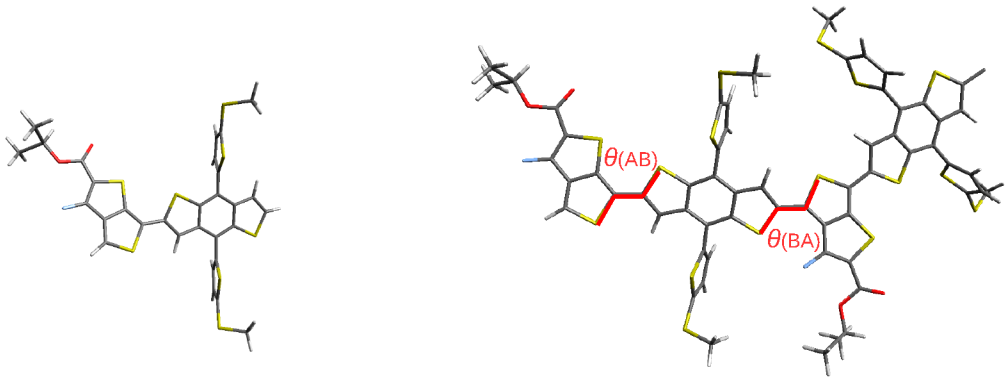

Figure 2.3: Atomic structure of the PBDT-TS1 polymer with the monomer unit (**AB**) (left) and two linked units (**AB AB**) (right). The conjugated segment limiting SCCS dihedral angles θ(**AB**) and θ(**BA**) are labelled.

We employ a partitioning schema using a cutoff angle θ_{SCCS}=60°. This yields a total number of 2037 segments with the sequences of subunits $\mathbf{A}_n\mathbf{B}_n$, $\mathbf{A}_n\mathbf{B}_{n-1}$ and $\mathbf{A}_{n-1}\mathbf{B}_n$ for $n \in [1, 8]$ (Fig. 2.4). The distributions show that long chains are less frequent, and sequences $\mathbf{A}_n\mathbf{B}_n$ with the same number of subunits **A** and **B** are more frequent than those with unequal number. A total of 12 polymer chains remain unchanged.

We regard every PPDI molecule as a single hopping site and define the centres of segments by local centres of subunits **A** and **B** (orange points) (Fig. 2.5). The distance vector $\mathbf{d}_{\mathrm{RCOM}}$ between two hopping sites is determined as follows. The centre of mass of the central two PBI units is determined for all PPDI molecules, neglecting the side chains attached to them. As every polymer segment can consist of several sub-units **A** and **B**, we can assign a centre of mass to every subunit using only the atoms located in the polymer backbone. For an intermolecular charge transfer rate including PBDT-TS1 segments, the minimal distance $\mathbf{d}_{\mathrm{RCOM}}$ between all subunits in donor and acceptor molecule is regarded as the charge transfer distance (Fig. 2.5).

The VOTCA-based kMC simulations include Marcus, Jortner or Weiss-Dorsey rates with λ^{in}, ΔE^{in}(PBE0/6-31G*), scaled intermolecular $|J_{\mathrm{AB}}|$ DIPRO/DFTB/3OB-3-1 to CDFT for $N^{\mathrm{NN}} = 12$, intramolecular $|J_{\mathrm{AB}}|$ and ΔE_{AB} employing CDFT/PBE/80Ry with Troullier-Martins norm-conserving pseudopotentials, λ^{out} (Eq. 228) and ΔE^{out}.

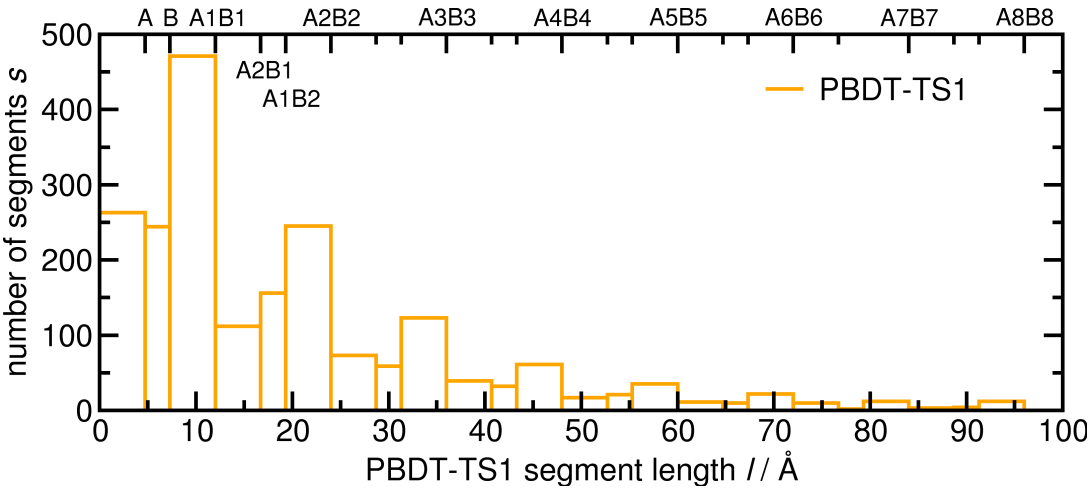

Figure 2.4: Distribution of PBDT-TS1 segments inside the blend morphology as a function of the segment length l. All 416 polymer chains are partitioned at a cutoff angle θ_{SCCS}=60°, which yields segments with the sequences $\mathbf{A}_n\mathbf{B}_n$, $\mathbf{A}_n\mathbf{B}_{n-1}$ and $\mathbf{A}_{n-1}\mathbf{B}_n$.

The partial charges are determined for PPDI and all possible $\mathbf{A}_n\mathbf{B}_n$ sequences $n \in [1, 8]$ with the CHelpG method on PBE0/6-31G* level in three electronic states. We evaluate E^{el} (Eq. 235) and E^{pol} (Eq. 241) within a cutoff $r_{\mathrm{cut}}^{\mathrm{out}} = 30$ Å. The kMC simulations for holes and electrons employ $N_{\mathrm{traj}} = 140$, $N_{\mathrm{steps}} = 1.0 \times 10^{10}$ at $F_i^{\mathrm{ext}} = 1 \times 10^7 \frac{\mathrm{V}}{\mathrm{m}}$ with $i \in x, y, z$. The Kondo parameter is set to $\alpha = 3.6$.

2.3 Screening for Polyene Diimide Acceptors

If not states explicitly in the text, we apply the following settings as a default. The DFT calculations were performed with the Gaussian 09 Rev. D.01 quantum chemistry package [251]. We perform DFT calculations on PBE0-D3(BJ)/6-31G* level, using the exchange-correlation functional PBE0 [101] along with Grimme's D3 dispersion correction with Becke-Johnson damping (BJ) [121] and the 6-31G* basis set. Alternatively, we apply the B3LYP hybrid functional [98, 99]. The geometries are optimised in the ground state S_0 followed by a frequency analysis calculation with Kohn-Sham density functional theory at a multiplicity $M = 1$. The UV-Vis absorption spectra were calculated using linear response TDDFT [68] for the lowest 80 singlet states. For better comparison to experimental data, a Lorentz broadening with a full width at half maximum (FWHM) of 15 nm was applied to the line spectra. The theoretical derived electronic circular dichroism spectra (ECD) [134, 274] are convoluted with a linewidth of 0.15 eV and normalised to match the experimental intensities. Solvent effects are taken into account using a polarisable continuum model (PCM) [275] with scaled Van der Waals radii for the solvation cavity from the universal force field (UFF) [276] treating hydrogen atoms explicitly. Methyl groups or hydrogen atoms can substitute the aliphatic side chains in order to reduce the computational coast. In case of several subsequent calculations, they are carried out at the same level of theory to ensure consistency.

We use B3LYP-D3(BJ)/6-31G* for **TPH**, **TPH-Se**, **PPD**, and **PPD-Se**. **HDI**, **TDI**, **NDI** and **PHHP-AS** are evaluated in chloroform solvent (PCM/UFF) on PBE0-D3(BJ)/6-31G* level. The ECD spectra are convoluted with a linewidth of 0.15 eV and normalised to match the experimental intensities.

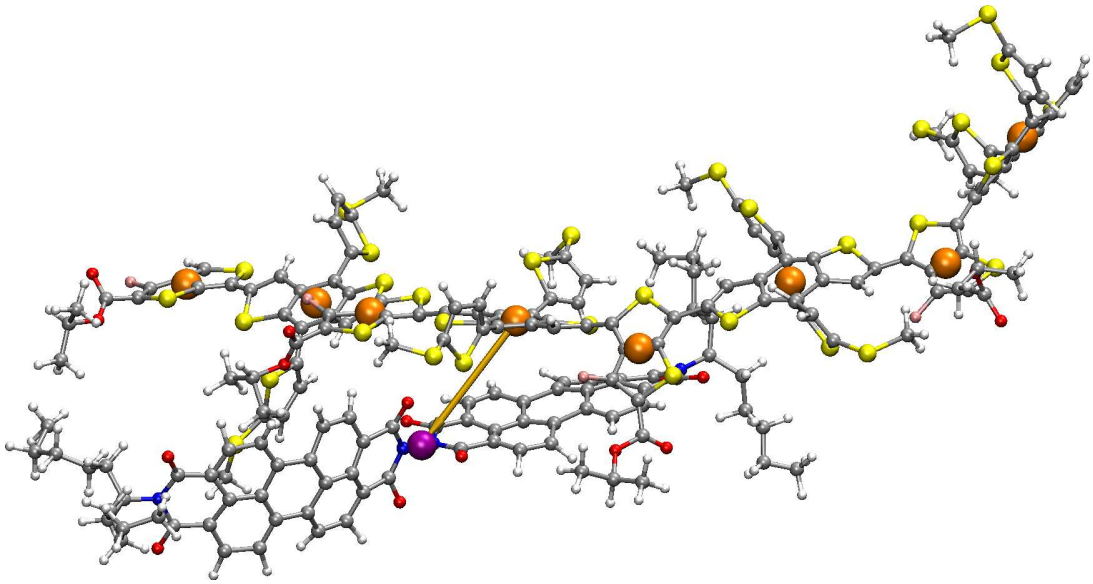

Figure 2.5: Visualisation of the intermolecular hopping site distance vector $\mathbf{d}_{\mathrm{RCOM}}$ (dark yellow line) between a PPDI molecule and a neighbouring PBDT-TS1 polymer chain segment. The PPDI hopping site centre is the molecular centre of mass (violet dot), excluding the aliphatic side chains. The PBDT-TS1 polymer chain segment comprises eight sub-units with a centre of mass located at the backbone of every subunit **A** and **B** (orange dots). The intermolecular hopping site distance is selected as the minimal distance $|\mathbf{d}_{\mathrm{RCOM}}|$=6.63 Å between the subunits and the PPDI hopping site.

PDTTI is evaluated in chloroform solvent (PCM/UFF) on PBE0-D3(BJ)/6-31G* level. The ECD are convoluted with a linewidth of 0.045 eV and normalised. The preliminary screening for the ECD calculations with various functionals (B3LYP, CAM-B3LYP, BH&HLYP, PBE0) shows the best results for PBE0.

Laddered nanoribbons: In PDI2-Pyr1 and PDI4-Pyr3 the aliphatic side chains are substituted by methyl groups, whereas in PDI8-Pyr7 the aliphatic side chains and the t-butyl groups were substituted by hydrogen atoms. The chloroform solvation cavity is modelled by PBE0-D3(BJ)/6-31G*/PCM using Van der Waals radii scaled with Bondi's model [265].

Dimers For comparability of the charge transfer rates, we perform all dimer calculations on B3LYP-D3(BJ)/6-31G* level, e.g. geometry optimisations, DIPRO-based charge transfer integrals $|J_{\mathrm{AB}}|$ and reorganization energies $\lambda_{\mathrm{AB}}^{\mathrm{in}}$ and energies $\Delta E_{\mathrm{AB}}^{\mathrm{in}}$. The electrostatic potential (ESP) maps of single molecules are calculated with an isovalue of 0.003 from the total electron density obtained by DFT at the neutral ground state geometry. The ESP maps aid to visualise possible intermolecular interaction sites. We align 5 to 10 pairs of molecules according to their electrostatic affinity and carry out geometry optimisations to generate different aggregation patterns for dimer structures. The reorganization energies require calculations of the adiabatic potential energy surface of the neutral and positively charged state for hole transfer and the negatively charged state for electron transfer in the framework of Marcus theory. The Marcus rates are evaluated at an external field $F^{\mathrm{ext}} = 1 \times 10^7 \frac{\mathrm{V}}{\mathrm{m}}$ using the COM distance at a temperature $T = 300$ K. Outer-sphere contributions are set to zero.

2.4 Charge Transfer in OLED Materials

The ab initio molecular dynamics (AIMD) simulations are carried out with the CPMD program package [252]. We use the PBE functional [100] in conjunction with a plane wave basis with a cutoff of 25 Ry and Vanderbilt ultrasoft pseudopotentials (USPP) [166]. Grimme's D2 dispersion correction [119] was employed for the dimers and trimers. The PCG algorithm was used to optimise the Kohn-Sham wavefunction to 1.0×10^{-5} a.u. and the BFGS algorithm [277, 278] for geometry optimisations to 1.0×10^{-4} a.u.. The size of the orthorhombic simulation box was $18.0 \times 14.0 \times 17.0$ Å^3 for the H-terminated **C3** complex (**C3-H**), $17.0 \times 12.0 \times 19.0$ Å^3 for **C5-H**, $23.0 \times 18.0 \times 14.0$ Å^3 for **D-C3-H**, $25.0 \times 18.0 \times 18.0$ Å^3 for **D-C5-H** and $25.0 \times 19.0 \times 22.0$ Å^3 for **T-C3-H** and **T-C5-H**.

The temperature was controlled by a Nosé-Hoover chain thermostat [182, 183] setting the target average to $T = 500$ K and the coupling frequency to the heat bath to 2500 cm^{-1}. All hydrogen atoms were replaced by deuterium permitting a timestep of $\Delta t = 7$ a.u. using a fictitious orbital mass of $\mu = 800$ a.u.. The overall simulation time was $t_{\max} = 4.23$ ps for the monomers and 8.46 ps for the dimers and trimers. At every restart after 5000 time steps, the electronic system was quenched to the Born-Oppenheimer adiabatic potential energy surface. The alkyl chains were replaced by hydrogen atoms in order to reduce the computational cost of the AIMD simulations, since they were shown to have a negligible effect on the spectral properties.

To obtain the averaged absorption spectrum of the monomers, we selected 30 geometries at regular intervals along the ground state trajectory, after an equilibration time of about 1 ps and performed TDDFT/PBE0/SDD calculations of the 40 lowest excited singlet states. A Gaussian broadening with a FWHM= 10 nm was used for each transition.

The emission spectra of the dimers were calculated from 50 snapshots along a T_1 trajectory. For each snapshot, the emission wavelength was obtained from the $T_1 \rightarrow S_0$ transition energy within TDDFT. The contributions of all 50 snapshots were weighted equally and a Gaussian broadening with a FWHM= 20 nm was applied for each transition.

We perform geometry optimisations in the S_0 and T_1 state on dimer structures using the PBE functional [100] in conjunction with a plane wave basis with an energy cutoff of 80 Ry and pseudopotentials by Goedecker, Teter, and Hutter (GTH) [279–281]. Moreover, we employ the local spin density approximation also in the subsequent calculations for $|J_{AB}|$ using CDFT.

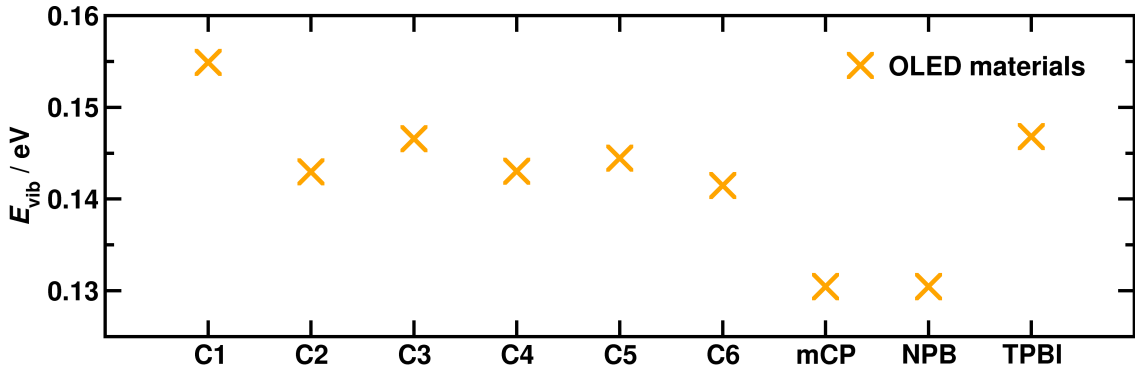

Figure 2.6: Average vibrational energy $E_{\text{vib}} = \hbar\overline{\omega}^{\text{int}}$ as contributions to the Jortner charge transfer rates for OLED materials, e.g. Pt complexes **C1** to **C6**, host material **mCP**, **NPB** and **TPBI**.

We compare charge transfer rates based on Marcus theory [189] to Jortner rates [207] and Weiss-Dorsey rates [202–204] with a Kondo parameter $\alpha = 3.6$ [201]. Figure 2.6 displays the applied average vibrational energies in Jortner rates for different OLED materials. Jortner rates on optimised **CX**/**mCP**, **CX**/**NPB** dimers include DIPRO-based $|J_{\mathrm{AB}}|$ (PBE0-D3(BJ)/SDD).

The binding energy E_{B} of the dimers in the ground state S_0 is evaluated at the PBE0-D3(BJ)/SDD level by subtracting twice the monomer energy E_{mono} from the dimer energy E_{dimer}. For the binding energy of the dimer in the T_1 state, one of the two monomers is considered to be in the T_1 state, the other in the S_0 state for comparison. Analogous formulae are used for the trimers.

$$E_{\mathrm{B}}(\mathrm{S}_0) = E_{\mathrm{dimer}}(\mathrm{S}_0) - 2\mathrm{E}_{\mathrm{mono}}(\mathrm{S}_0) \tag{269}$$

$$E_{\mathrm{B}}(\mathrm{T}_1) = E_{\mathrm{dimer}}(\mathrm{T}_1) - \mathrm{E}_{\mathrm{mono}}(\mathrm{T}_1) - \mathrm{E}_{\mathrm{mono}}(\mathrm{S}_0) \tag{270}$$

$$E_{\mathrm{B}}(\mathrm{S}_0) = E_{\mathrm{trimer}}(\mathrm{S}_0) - 3\mathrm{E}_{\mathrm{mono}}(\mathrm{S}_0) \tag{271}$$

$$E_{\mathrm{B}}(\mathrm{T}_1) = E_{\mathrm{trimer}}(\mathrm{T}_1) - \mathrm{E}_{\mathrm{mono}}(\mathrm{T}_1) - 2\mathrm{E}_{\mathrm{mono}}(\mathrm{S}_0) \tag{272}$$